A Lithium-Sulfur Battery with a High Areal Energy Density

*Joo-Seong Kim, Tae Hoon Hwang, Byung Gon Kim, Jaeyun Min, and Jang Wook Choi**

The battery community has recently witnessed a considerable progress in the cycle lives of lithium-sulfur (Li-S) batteries, mostly by developing the electrode structures that mitigate fatal dissolution of lithium polysulfides. Nonetheless, most of the previous successful demonstrations have been based on limited areal capacities. For realistic battery applications, however, the chronic issues from both the anode (lithium dendrite growth) and the cathode (lithium polysulfide dissolution) need to be readdressed under much higher loading of sulfur active material. To this end, the current study integrates the following three approaches in a systematic manner: 1) the sulfur electrode material with diminished lithium polysulfide dissolution by the covalently bonded sulfur-carbon microstructure, 2) mussel-inspired polydopamine coating onto the separator that suppresses lithium dendrite growth by wet-adhesion between the separator and Li metal, and 3) addition of cesium ions (Cs^+) to the electrolyte to repel incoming Li ions and thus prevent Li dendrite growth. This combined strategy resolves the long-standing problems from both electrodes even under the very large sulfur-carbon composite loading of 17 mg cm^{-2} in the sulfur electrode, enabling the highest areal capacity (9 mAh cm^{-2}) to date while preserving stable cycling performance.

1. Introduction

Upcoming advanced portable electronic devices and green transportation require advent of lithium ion batteries (LIBs) with higher energy densities. The increasing demand on the higher energy density LIBs has driven the battery community to investigation of active electrode materials whose specific capacities can go beyond those of the conventional intercalation-based ones represented by graphite[1] and lithium metal oxides (i.e., $LiCoO_2$[2] and $LiMn_2O_4$).[3,4] Among such candidates functioning based on new redox chemistry, lithium-sulfur (Li-S) batteries have received discernable attention due to their unparalleled energy densities. The theoretical specific capacity of sulfur (=1675 mAh g^{-1}) allows the Li-S cell to reach 2567 Wh kg^{-1} for its theoretical energy density, which is approximately 6.6 times larger than that of the current intercalation-based LIBs (≈387 Wh kg^{-1}).[5–8]

Remarkably, recent research efforts have been successful in resolving the chronic technical challenges associated with sulfur electrodes, especially dissolution of lithium polysulfides and low electric conductivity of elemental sulfur.[9–12] The representative solutions along this direction include sulfur-carbon composite structures that minimize sulfur exposure to electrolyte,[5,13] surface coating of active particles,[7,14–16] engagement of allotropic sulfur,[17,18] and use of solid-state electrolytes[19] and electrolyte additives.[20,21] Although the improved cycle lives based on these approaches represent considerable progresses in the area of Li-S batteries, it should be noted that the most critical issue related to Li metal anodes still remains unaddressed: upon repeated charge and discharge, Li dendrites grow on the surface of the Li metal anode, which triggers multiple mechanisms for rapid capacity fading. The electrolyte becomes decomposed successively along the Li dendrite surfaces, which destabilizes the electrode-electrolyte interface and also increases the resistance (or overpotential) leading to continuous capacity decay. The electrolyte could be eventually exhausted. The dendrite growth could also promote short circuits between both electrodes, and thus resulting in severe safety hazard.[22] An additional but very critical hurdle related to the Li dendrite growth is that the dendrite growth becomes accelerated with areal current density.[22–26] Hence, the increase in the areal capacity of sulfur electrode (or the areal mass loading of sulfur active material) would amplify the problems originating from Li dendrites. Likewise, the dissolution of the fatal lithium polysulfides would also be amplified under the increased areal capacity. The demonstration of improved cycle lives from most of recent sulfur electrode designs, in turn, implies that the cycling tests were conducted with moderate mass loadings of the sulfur active materials. Therefore, in order to exalt Li-S batteries to more practical technology, more systematic approaches need to be engaged to resolve the issues from both sides of electrodes.

With purpose of developing Li-S cells with high areal energy densities, herein, we have adopted or discovered the key cell components (sulfur electrode, separator, and electrolyte) in a way that Li dendrite formation and polysulfide dissolution are minimized even at a practically viable loading of sulfur active material (≈17 mg cm^{-2}, the mass of sulfur-carbon composite). The synergistic outcomes from smart engineering of each

J.-S. Kim,[+] T. H. Hwang,[+] B. G. Kim, J. Min, Prof. J. W. Choi
Graduate School of Energy, Environment Water and Sustainability (EEWS) and Center for Nature-inspired Technology (CNiT)
KAIST Institute NanoCentury
Korea Advanced Institute of Science and Technology (KAIST)
291 Daehakro, Yuseong-gu, Daejeon 305-701, Republic of Korea
E-mail: jangwookchoi@kaist.ac.kr

[+]J.-S. K. and T. H. H. contributed equally to this work

DOI: 10.1002/adfm.201400935

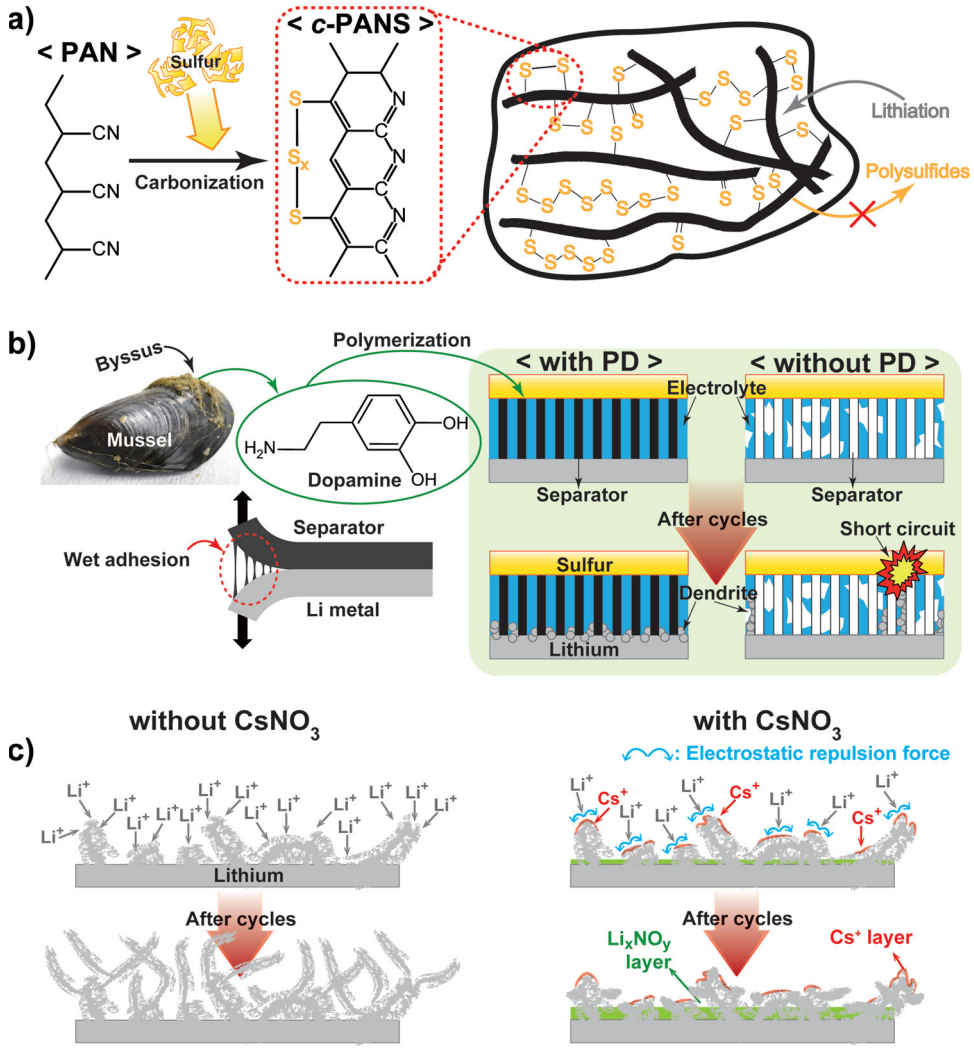

Figure 1. The main strategies for the Li-S cell with a large areal capacity. a) The synthetic procedure and molecular structure of the cathode active material, *c*-PANS. b) Mussel-inspired polydopamine coating onto the separator to mitigate Li dendrite growth via uniform Li ionic flux and wet-adhesion. c) Addition of $CsNO_3$ in the electrolyte to suppress Li dendrite growth by electrostatic repulsion between Cs^+ ion and incoming Li^+ ion. NO_3^- also contributes to formation of stable interfacial layer on the Li metal anode.

component allow the areal capacity to reach the highest value (≈9 mAh cm^{-2}) to date along with decent cyclability (73.3% capacity retention after 90 cycles). The demonstration of the high performance Li-S cell even at such high areal capacity conveys a promising message that the longstanding chronic issues in the Li-S battery technology could be resolved to meet the commercial standards once systematic approaches are incorporated.

2. Results and Discussions

Figure 1 schematically illustrates our strategy with regard to each key component:

1. Since it has been widely accepted that long chain lithium poly sulfides (Li_2S_x, $2 < x \leq 8$)[6,18,27] soluble into the electrolyte give rise to the shuttling effect that triggers fatal capacity fading, we have adopted the C-S structure as a sulfur cathode where short chains of elemental sulfur are covalently bonded to carbon matrix (Figure 1a). This C-S structure can be synthesized through a simple procedure: commercially available polyacrylonitrile (PAN) was thoroughly mixed with elemental sulfur powder in a mass ratio of 2:8, and the PAN-derived C-S composite was then completed by a carbonization step at 450 °C for 6 h under nitrogen atmosphere. The final carbonized C-S structure is denoted *c*-PANS. See the Experimental Section for detailed experimental procedures.
2. In order to suppress Li dendrite growth, mussel-inspired polydopamine (PD) was coated onto separator because PD can be uniformly coated onto a wide range of surfaces[28] including polyethylene, the material of separator in the current investigation, and can thus facilitate uniform Li ionic flux during battery operations through enhanced wetting with the electrolyte, 1.15 M of lithium bis(trifluoromethanesulfonyl) imide (LiTFSI) dissolved in dioxolane/dimethoxyethane

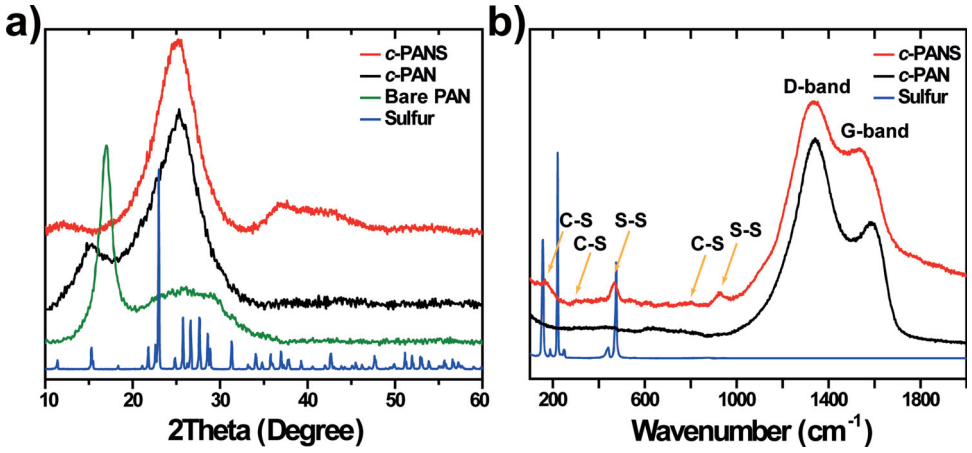

Figure 2. a) The XRD and b) Raman spectra of *c*-PANS, *c*-PAN, PAN, and elemental sulfur.

co-solvents (DOL/DME, v/v = 1:1). The poor wetting of electrolyte with the separator results in locally concentrated Li ion flux that accelerates Li dendrite growth. Beside the uniform ionic flux,[29–31] the wet-adhesion[30,32] of mussel-inspired PD enables molecule-level contacts between the separator and Li metal electrode, which also assists the inhibition of Li dendrite growth by diminishing surface tension of Li metal.[30]

3. As another attempt to prevent Li dendrite growth, cesium nitrite ($CsNO_3$) was included in the electrolyte. Cs ions at controlled concentrations, 0.05 M in our case, can stay in the positively charged ionic state[25] even at the potentials where Li^+ ions are reduced to Li^0. In particular, ionic state Cs tends to migrate toward sharp morphological spots on the Li metal surface where electrons are more heavily concentrated. The Cs ions at these sharp spots electrostatically repel the incoming Li ions and thus hinder further deposition of Li metal at the spots where Li dendrites would grow otherwise.[23,25,26]

Once again, the synergistic consequences from these three efforts address the critical issues from both sides of the electrodes all at once and allow for stable cycling of a Li-S cell with the markedly increased areal capacity.

Various analyses (**Figures 2** and S1–S2, Supporting Information) indicate two main characteristics of *c*-PANS with respect to its atomic structure: graphitic atomic structure of the carbon matrix and short sulfur chains covalently bonded to the carbon matrix. Elemental sulfur (S_8), bare PAN, and carbonized PAN (*c*-PAN) were also characterized together as control samples. The graphitic character of *c*-PANS was first revealed by X-ray diffraction (XRD) spectra (Figure 2a). *c*-PANS exhibited a broad peak at $2\theta = 24.4°$ corresponding to the graphitic (002) plane,[33,34] which is in contrast with *c*-PAN that exhibited an additional peak at $2\theta = 15°$ reflective of residual bare PAN[34,35] and therefore lesser degree of graphitization. The enhanced graphitization of *c*-PANS is associated with the role of sulfur as a catalyst[36–40] for dehydrogenation of PAN, which facilitates efficient π-π interactions between carbon layers. Also, the Raman spectroscopic data (Figure 2b) showing increased G-to-D peak ratio (I_G/I_D) between *c*-PANS and *c*-PAN additionally support the higher graphitization by the reaction with sulfur.

The formation of C-S bonds was evidenced by series of analytical results. 1) Aside the increased I_G/I_D, the Raman spectrum (Figure 2b) of *c*-PANS showed the C-S peaks at 171, 301, and 803 cm^{-1}, which are absent in the *c*-PAN counterpart. 2) Similarly, the FT-IR data (Figure S1a) exhibited peaks at 673 and 941 cm^{-1} assigned to the C-S bonds. 3) Thermal gravimetric analysis (TGA) result of *c*-PANS (Figure S1b) showed a negligible weight loss of ≈3.88% up to 600 °C in spite of a sulfur content of 39.62 wt% according to elemental analysis (EA) result (Figure S2c, Supporting Information). This result reconfirms the strong covalent bonding of sulfur with the carbon matrix. The results from the structural analyses of *c*-PANS are consistent[36–40] with those reported previously and are discussed more in detail in the Supporting Information.

Next, the effect of PD-coating onto the separator was investigated when *c*-PANS was used as a cathode active material. In **Figure 3**, the scanning electron microscope (SEM) images on the left column (Figures 3a–d) are top-views of the Li metals when the PD-coating was engaged, and those on the right column (Figures 3e–h) are for the opposite cases. In both columns, a general trend is that as the current density increases, the morphology of the Li metal becomes sharper. This observation is commensurate with the early works by the Aurbach,[22] Zhang,[23] and Fukunaka[24] groups that found amplified Li dendrite growth proportionally to the charging current density. Even between both columns, however, the cases with the PD-coating exhibited more controlled dendrite growth. At the same current densities, the images with the PD-coating clearly showed more rounded and suppressed morphologies for Li dendrites. While the more rounded morphology can be explained by uniform Li ionic flux by the improved wetting with the electrolyte, the more suppressed morphology reflects the wet adhesion between the separator and Li metal.

In an effort to mitigate the Li dendrite growth further, $CsNO_3$ was added in the electrolyte as an additive. The addition of $CsNO_3$ is dual-purposed: As described in Figure 1c, Cs ions are expected to remain positively charged even at the voltages where Li ions are reduced to zero-valent Li. The presence of the positively charged Cs ions electrostatically repels Li ions and thus prevents deposition of Li metal, especially at sharp tips on the Li surface where electron densities are higher than other locations

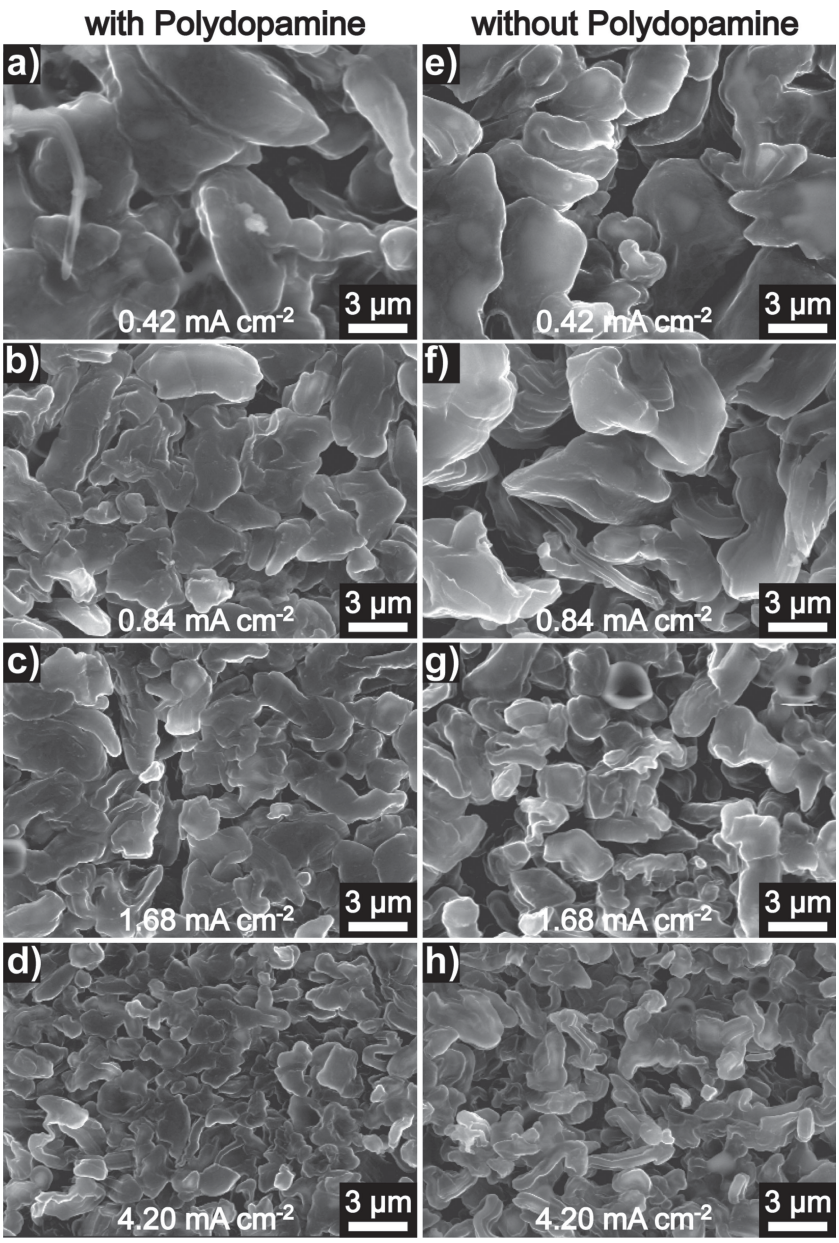

Figure 3. SEM images of the top-viewed Li metal after 3 deep cycles when measured at various current densities in the potential range of 1.0–3.0 V vs. Li/Li^+. For the cases with the PD-coating on the separators at a) 0.42 mA cm^{-2}, b) 0.84 mA cm^{-2}, c) 1.68 mA cm^{-2}, and d) 4.20 mA cm^{-2}. e–h) For the same cases but without the PD-coating on the separators. In the case of 4.20 mA cm^{-2}, each charge and discharge takes 2 h.

with flat morphology. On the other hand, NO_3^- was chosen as a counterion because NO_3^- has been known[7,8,13,20,21] to assist forming stable interfacial layers on Li metal surface in Li-S cells. To see this electrolyte additive effect, the samples were divided into two cases with and without the PD-coating on the separator. From comparative evaluation of macroscopic photographs and SEM images after 3 deep cycles (**Figure 4**), it appears that the additive effect is more dramatic than the PD-coating effect. After the same 3 cycles at 0.84 mA cm^{-2}, the morphology sharpness was more pronounced in the sequence of $CsNO_3$, $LiNO_3$, and no additive. In particular, the $CsNO_3$ sample showed significantly lessened Li dendrite growth in conjunction with far more rounded morphology of each dendrite, verifying the Cs ion effect. In addition, it is noteworthy that $CsNO_3$ is commercially available and cost-effective. As in Figure 3, the PD-coating turned out to affect the microscopic morphologies of Li dendrites towards more rounded and suppressed morphology again due to the wet adhesion between the separator and Li metal. Furthermore, the thickness of Li metal dendrite reflects the dramatic effects of the additive and the separator coating. For the PD-coated cases (Figure 4c), the samples with no additive, $LiNO_3$, and $CsNO_3$ showed the Li dendrite thicknesses of 75, 20, and 2 μm, respectively. For the cases without the PD-coating (Figure 4d), the thicknesses were greater such as 115, 25, and 6 μm for the three corresponding cells, respectively. Interestingly, when both additives were included in the electrolyte, dark spots were observed (Figures 4a and b). According to X-ray photoelectron spectroscopy (XPS) analyses (Figure S3, Supporting Information), these black spots are Li_3N, and its formation is seemingly associated with decomposition of $LiN(SO_2CF_3)_2$ (LiTFSI) and NO_3^-,[21] the common anion in both additives. These black spots appeared mostly on top of Li dendrites over the center region of the Li metal piece where the electron density is relatively higher. Also, the formation of the interfacial layers in the presence of NO_3^- was reflected in the discharge voltage profiles that showed short plateaus around 1.7 V (Figure S4, Supporting Information).

The effects of the PD-coating and electrolyte additives on the electrochemical performance were assessed by galvanostatic measurements. For this testing, coin-type cells containing the *c*-PANS electrodes consisting of *c*-PANS, denka black, and styrene-butadiene rubber/carboxymethyl cellulose (SBR/CMC) binder in a weight ratio of 80:10:10 along with Li metal foil were prepared. From this electrode composition and the aforementioned sulfur content (39.62 wt%) in *c*-PANS, sulfur accounts for ≈32 wt% of the entire electrode. Although more than a certain content of sulfur should be included to take full advantage of its high capacity,[41,42] we had to choose *c*-PANS for the given high areal capacity (≈9 mAh cm^{-2}) because most of other sulfur electrodes would not be functional at such large loadings due to amplified lithium polysulfide dissolution. Detailed material information, cell assembly procedure, and measurement conditions are described in the Experimental Section. From the cycling performance results (**Figure 5**), the following points are remarkable:

First, in agreement with the morphology results (Figure 4), it was found that the electrolyte additive has much more impact on

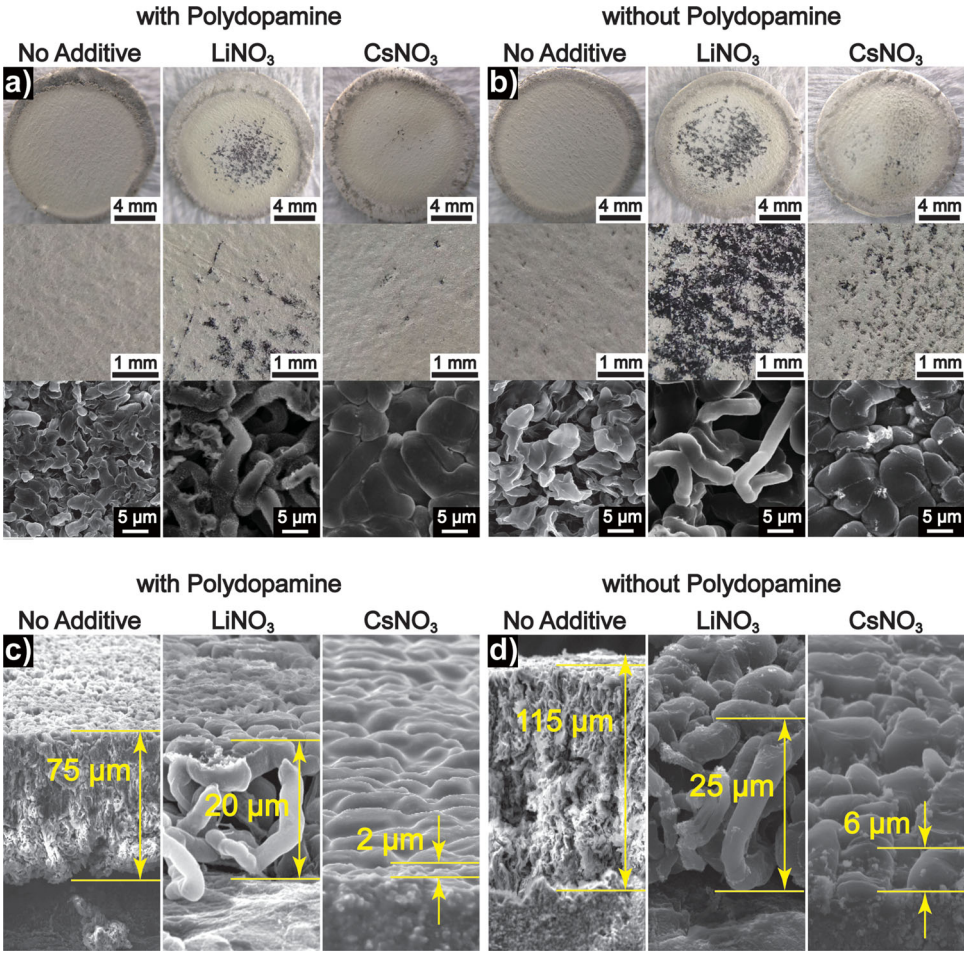

Figure 4. a) SEM and digital photograph images of the top-viewed Li metal after 3 deep cycles for the cases of the PD-coated separators when no additive, $LiNO_3$, and $CsNO_3$ were added to the electrolytes. All of the cells were cycled at 0.84 mA cm^{-2} in the potential range of 1.0–3.0 V vs. Li/Li^+. b) For the same cases but without the PD-coating on the separators. c,d) The cross-sectional SEM images for the same samples in (a,b) to show the distinct Li dendrite thicknesses.

the cycling performance than the PD-coating on the separator. In the cases of the PD-coated separators (Figure 5a), the electrolytes with $CsNO_3$, $LiNO_3$, and no additive exhibited distinctive capacity retentions of 74.1%, 56.7%, and 34.4% after 90 cycles, respectively, with respect to their initial capacities, revalidating the critical role of Cs ions for the cycling performance. It needs to be emphasized that the 73.3% capacity retention after 90 cycles is quite noticeable considering that the original areal capacity and

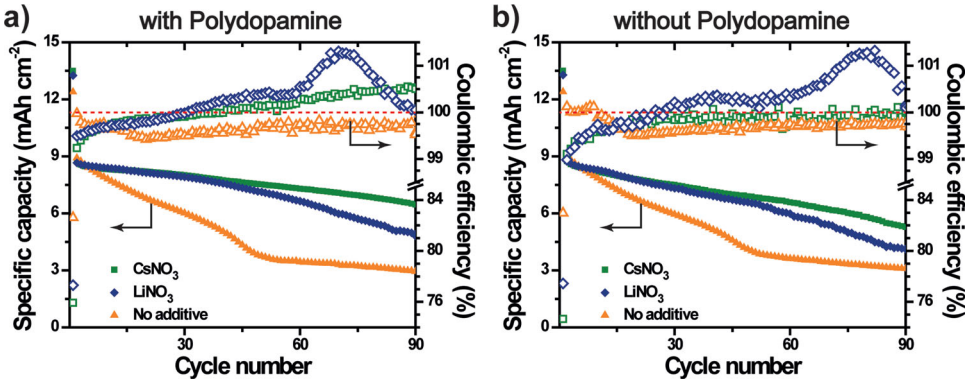

Figure 5. The discharging capacity retentions and Coulombic efficiencies of the *c*-PANS/Li cells with the various electrolyte additives for the cases (a) with and (b) without the PD-coating onto the separators. In both figures, all of the cells were measured at 0.42 mA cm^{-2} for charge and 4.2 mA cm^{-2} for discharge under the CC mode in the potential range of 1.0~3.0 V vs. Li/Li^+.

mass loading of the active material are unprecedentedly high: ≈9 mAh cm^{-2} and ≈17 mg cm^{-2}. Since both Li dendrite growth and lithium polysulfide dissolution take place simultaneously, it is difficult to isolate the effect of each fading mechanism. However, it can be speculated that the Li dendrite growth is a more dominant fading mechanism according to the SEM images in Figure 4, especially in the condition that the identical *c*-PANS electrodes were used for all the additive cases. $LiNO_3$ could play a role in lessening the shuttling effect,[6–8,10,13,20,21] but its role against the Li dendrite growth must also be significant in our experimental conditions based on the high current densities.

Second, the PD-coating on the separator contributes to preservation of the original capacity, as the same cells but without the PD-coating exhibited lower capacity retentions of 60.4%, 47.1%, and 33.1% after 90 cycles operated in the same conditions (Figure 5b). The improved cycling performance by the electrolyte additive and PD-coating reflects once again the critical nature of controlling Li dendrite growth.

Finally, the trend of Coulombic efficiency (CE), defined as charge capacity/discharge capacity, appears to be closely related to that of the capacity retention because the capacity fading started drastically at the point where the CE surpasses 100%. In Figure 5a, the CEs of the no additive, $LiNO_3$, and $CsNO_3$ samples surpassed at the 2nd, 31st, and 41st cycle, respectively. These phenomena can be explained by the fact that the cycle life becomes destabilized when the charge capacity exceeds the discharge capacity, and this circumstance is attributed to the side reactions at the Li metal interface during the charge originating from the Li dendrite growth and lithium polysulfide dissolution. Since the no additive sample reached this critical point even in the very early period of the cycles and started to show the capacity fading, the Li dendrite formation is ascribed as a more dominant origin for the capacity fading. The lithium polysulfide dissolution would not be serious only for this sample, but is rather expected to be similar for all of the three samples. Thus, the CE can be a good indicator on the cycle life of the Li-S cell. In addition, the lower CEs in the first cycles are attributed to Li ion trapping in the *c*-PANS structure, wherein a certain structural rearrangement takes place by breaking the original C-S and S-S bonds of *c*-PANS and forming Li-S bonds.[43]

The best performing cell engaging the $CsNO_3$ additive and PD-coating was examined further focusing on rate capability and high temperature tolerance (**Figure 6**). Even when the current density increased by 20 times (0.42–8.4 mA cm^{-2}), the *c*-PANS/Li cell exhibited a decent capacity retention of 82.8% at 25 °C, indicating efficient Li diffusion in *c*-PANS. The high degree graphitization of *c*-PANS supporting electronic conductivity within the active material and the improved wetting of the separator by the PD-coating supporting Li ion diffusion must play an important role in the observed rate performance. This rate capability was maintained at a higher temperature of 55 °C, implying that the electronic/ionic transport in the *c*-PANS electrode is not very much sensitive to temperature in the typical temperature range of battery operations. However, the voltage profiles at both temperatures (Figures 6b and c) indicate that the overpotential decreased clearly at the higher temperature, reflecting that there exist some activation barriers for Li diffusion during charge and discharge, and Li (de)insertion into *c*-PANS must be one of the most relevant processes for the activation barriers.

The cell containing the $CsNO_3$ additive and PD-coating also exhibited decent cycling performance at 55 °C. Up to 75 cycles, the cell showed almost same capacities and capacity retention as compared to those at 25 °C. The similar capacities indicate that the *c*-PANS electrode is substantially activated even at room temperature. On the other hand, the similar capacity retention until a considerable number of cycles suggests that side reactions on the Li metal dendrites on the anode side[24] and the polysulfides dissolution from the cathode side, both of which would be amplified at higher temperatures, are indeed suppressed quite a bit by involving the aforementioned three strategies. It was, however, still observed that the cell at 55 °C began to lose the capacity distinctively after ≈78 cycles, from which it can be concluded that there is still a certain room for further improvement towards complete prevention of Li dendrite growth at high temperatures. In particular, it is likely that the Li dendrite growth plays a critical role in the inferior cycling performance at the higher temperature since it has been known[24] that with the temperature increase, the dendrite growth is accelerated with morphology evolution toward sharp needle-like shapes. The increased overpotentials with cycling in Figures 6e,f are also reflective of the continuous Li dendrite growth, although the lithium polysulfide dissolution would also contribute to such increase to some extent.

It would be instructive to compare the areal capacity (≈9 mAh cm^{-2}) in the present study with those of existing commercial LIB cells. For example, typical areal capacities of LIBs used for IT, hybrid electrical vehicle (HEV), and electrical vehicle (EV) applications are ≈3.5, ≈0.8, and ≈3.0 mAh cm^{-2}, respectively (Table S1, Supporting Information). Even after consideration of the operating voltage, the areal energy density of the present cell was found to be substantially higher than those of the aforementioned three representative LIB applications (15.3 vs 12.9, 3.0, 11.1 Wh cm^{-2}, respectively). For these calculations, 1.7 V and 3.7 V were used as the operating voltages in our and the conventional LIB cases, respectively. Furthermore, even under such high loading condition, the gravimetric capacity of *c*-PANS reached ≈1080 mAh g^{-1} at 8.40 mA cm^{-2} when only sulfur, not *c*-PANS, content was counted. This excellent value is again attributed to the well-developed carbon matrix in *c*-PANS originating from the π-π interaction of PAN.

3. Conclusion

The current investigation suggests that once smart engineering approaches are incorporated for the key cell components, the chronic issues of Li-S cell can be resolved even at the areal energy density higher than those of commercial LIBs. Since the present Li-S cell could deliver high gravimetric energy density as well, the decent cell performance demonstrated herein must be meaningful for diverse applications where the gravimetric energy densities are critical. The present study also indicates that other cell components than sulfur electrode should be tailored in parallel to upgrade the existing Li-S batteries to a commercially viable technology.

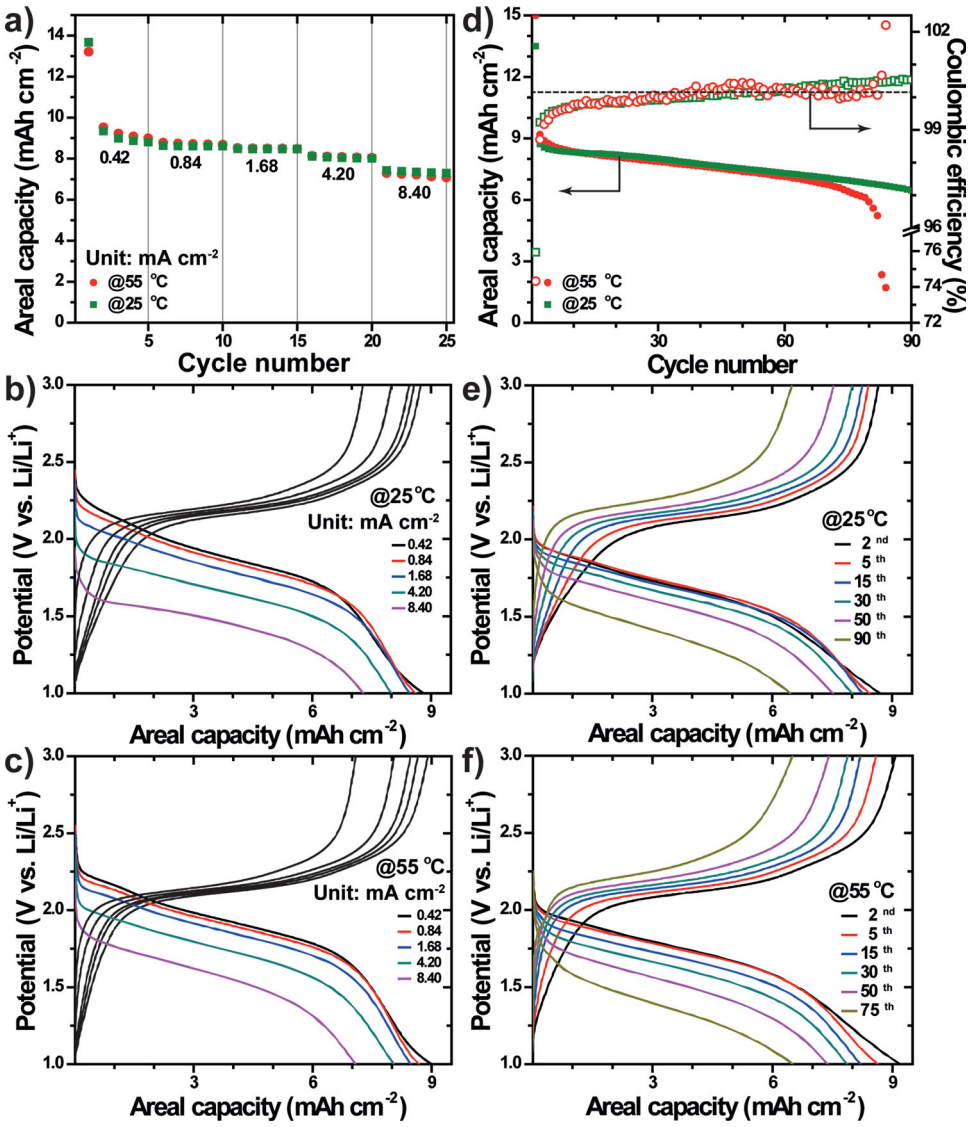

Figure 6. Electrochemical performance of the *c*-PANS/Li cell with the $CsNO_3$ additive and PD-coating at 25 and 55 °C. a) Summarized rate capability. The corresponding voltage profiles at various current densities at b) 25 °C and c) 55 °C. d) Capacity retentions and Coulombic efficiencies at both temperatures when measured at 0.42 mA cm^{-2} for charge and 4.20 mA cm^{-2} for discharge in the potential range of 1.0–3.0 V vs. Li/Li^+. The corresponding voltage profiles at different cycle numbers at e) 25 °C and f) 55 °C.

4. Experimental Section

4.1. Material Synthesis of *c*-PANS

For synthesis of *c*-PANS, 12.5 g of polyacrylonitrile (PAN, M_w = 150 000, Aldrich) and 50 g of elemental sulfur (Aldrich) were first homogeneously mixed by a ball-milling process at 300 rpm for 12 h. The mixed sample was transferred into a tube furnace and heat-treated at 450 °C for 6 h under N_2-flow at 500 sccm. The heating rate was 10 °C min^{-1}. Finally, the synthesized *c*-PANS powder was ground using a mortar and pestle for 30 min.

4.2. Characterization of *c*-PANS

The crystal structures of the electrode materials were analyzed by X-ray diffraction (XRD, Rigaku). The chemical bond characteristics of each compound were investigated by Raman spectroscopy (Horiba Jobin Yvon) equipped with a He-Ne laser with 633 nm wavelength. To identify vibration characters, the samples were analyzed by Fourier transform infrared spectroscopy (FT-IR, Bruker) by preparing KBr pellets. The thermal stability and sulfur contents of the samples were investigated using a thermogravimetric analyzer (TGA, Netzsch) and an element analyzer (EA, Thermoquest Italia S.P.A). The microscopic

morphology of Li metal was investigated by field emission scanning electron microscope (FE-SEM, Sirion).

4.3. Polydopamine-coating Onto Polyethylene Separator

The PD-coated polyethylene (PE) separators (SK innovation Co., Ltd.) were prepared by simple immersion of the separators into the dopamine hydrochloride solution in co-solvents (18 mM, methanol (MeOH):Tris buffer solution (pH = 8.5) = 1:1 = v/v).[29,30] After 24 h, dopamine was polymerized into polydopamine while coating the separators uniformly. The coated separators were washed with deionized water and MeOH several times. Finally, the separators were dried at 70 °C in a vacuum oven for 24 h. The mass increase of the separator after the polydopamine-coating was 6% with respect to the original value.

4.4. Cell Preparation and Electrochemical Measurements

The sulfur electrodes were prepared based on the following procedure: *c*-PANS, denka black, and SBR/CMC binder were dispersed in water in a weight ratio of 80:10:10. The loading of *c*-PANS was 17 mg cm^{-2}, and by consideration of its sulfur content (39.62 wt%) the pure sulfur loading was 6.74 mg cm^{-2}. Using the doctor blade method, the well-mixed slurry was cast onto the Ni-coated conductive polyester textile described in the previous study.[44,45] The mass increase of the textile after the Ni-coating was ~83% with respect to the original value. The Ni-coated textile current collector was chosen instead of aluminum foil because the aluminum foil often suffered from crack formation and film delamination (Figure S5) when the given loading of *c*-PANS was involved. By contrast, the Ni-coated textiles did not experience such problems presumably due to its three-dimensional (3D) structures that can release the stress and enhance the adhesion. It is also notable that the Ni-coated textiles have sheet resistances around 0.35 Ω sq^{-1}, which is in the same order as those of most metal films. The electrochemical performance was characterized by preparing coin-type cells (CR2032). In these cells, 1.15 M LiTFSI (no additive cell) or 1 M LiTFSI and 0.15 M $LiNO_3$ ($LiNO_3$ cell) or 1 M LiTFSI and 0.1 M $LiNO_3$ and 0.05 M $CsNO_3$ ($CsNO_3$ cell) dissolved in co-solvents of DOL/DME (1:1 = v/v, PANAX ETEC, Korea) was used as electrolyte, and Li foil (Honjo Chemical Co.) was used as the anode. The entire cell assembly was carried out in an argon-filled glovebox. The electrochemical measurements were performed in the battery potential range of 1.0–3.0 V (vs. Li/Li^+) using a battery cycler (MACCOR series 4000) at different current densities at 25 °C and 55 °C. In each cycle, the charging and discharging processes were under the constant current (CC) mode.

Supporting Information

Supporting Information is available from the Wiley Online Library or from the author.

Acknowledgements

This work was supported by the National Research Foundation of Korea (NRF) Grant funded by the Korea government (MEST) (NRF-2010-C1AAA001–0029031 and NRF-2012-R1A2A1A01011970).

Received: March 22, 2014
Revised: April 20, 2014
Published online: June 23, 2014

[1] R. Yazami, P. Touzain, *J. Power Sources* **1983**, *9*, 365.
[2] K. Mizushima, P. C. Jones, P. J. Wiseman, J. B. Goodenough, *Mater. Res. Bull.* **1980**, *15*, 783.
[3] M. M. Thackeray, W. I. F. David, P. G. Bruce, J. B. Goodenough, *Mater. Res. Bull.* **1983**, *18*, 461.
[4] J.-S. Kim, K. Kim, W. Cho, W. H. Shin, R. Kanno, J. W. Choi, *Nano Lett.* **2012**, *12*, 6358.
[5] X. Ji, K. T. Lee, L. F. Nazar, *Nat. Mater.* **2009**, *8*, 500.
[6] Y.-S. Su, A. Manthiram, *Nat. Commun.* **2012**, *3*, 1166.
[7] Z. Wei Seh, W. Li, J. J. Cha, G. Zheng, Y. Yang, M. T. McDowell, P.-C. Hsu, Y. Cui, *Nat. Commun.* **2013**, *4*, 1331.
[8] P. G. Bruce, S. A. Freunberger, L. J. Hardwick, J.-M. Tarascon, *Nat. Mater.* **2012**, *11*, 19.
[9] H.-J. Peng, J.-Q. Huang, M.-Q. Zhao, Q. Zhang, X.-B. Cheng, X.-Y. Liu, W.-Z. Qian, F. Wei, *Adv. Funct. Mater.* **2014**, *24*, 2772.
[10] J. Song, T. Xu, M. L. Gordin, P. Zhu, D. Lv, Y.-B. Jiang, Y. Chen, Y. Duan, D. Wang, *Adv. Funct. Mater.* **2014**, *24*, 1243.
[11] G. Zhou, S. Pei, L. Li, D.-W. Wang, S. Wang, K. Huang, L.-C. Yin, F. Li, H.-M. Cheng, *Adv. Mater.* **2014**, *26*, 625.
[12] J. Guo, Y. Xu, C. Wang, *Nano Lett.* **2011**, *11*, 4288.
[13] G. Zheng, Y. Yang, J. J. Cha, S. S. Hong, Y. Cui, *Nano Lett.* **2011**, *11*, 4462.
[14] K. T. Lee, R. Black, T. Yim, X. Ji, L. F. Nazar, *Adv. Energy Mater.* **2012**, *2*, 1490.
[15] F. Wu, J. Chen, L. Li, T. Zhao, R. Chen, *J. Phys. Chem. C* **2011**, *115*, 24411.
[16] C. Nan, Z. Lin, H. Liao, M.-K. Song, Y. Li, E. J. Cairns, *J. Am. Chem. Soc.* **2014**, *136*, 4659.
[17] S. Xin, L. Gu, N.-H. Zhao, Y.-X. Yin, L.-J. Zhou, Y.-G. Guo, L.-J. Wan, *J. Am. Chem. Soc.* **2012**, *134*, 18510.
[18] S. Moon, Y. H. Jung, W. K. Jung, D. S. Jung, J. W. Choi, D. K. Kim, *Adv. Mater.* **2013**, *25*, 6547.
[19] Z. Lin, Z. Liu, N. J. Dudney, C. Liang, *ACS Nano* **2013**, *7*, 2829.
[20] X. Liang, Z. Wen, Y. Liu, M. Wu, J. Jin, H. Zhang, X. Wu, *J. Power Sources* **2011**, *196*, 9839.
[21] D. Aurbach, E. Pollak, R. Elazari, G. Salitra, C. S. Kelley, J. Affinito, *J. Electrochem. Soc.* **2009**, *156*, A694.
[22] D. Aurbach, E. Zinigrad, Y. Cohen, H. Teller, *Solid State Ionics* **2002**, *148*, 405.
[23] F. Ding, W. Xu, X. Chen, J. Zhang, Y. Shao, M. H. Engelhard, Y. Zhang, T. A. Blake, G. L. Graff, X. Liu, J.-G. Zhang, *J. Phys. Chem. C* **2014**, *118*, 4043.
[24] T. Nishida, K. Nishikawa, M. Rosso, Y. Fukunaka, *Electrochim. Acta* **2013**, *100*, 333.
[25] F. Ding, W. Xu, G. L. Graff, J. Zhang, M. L. Sushko, X. Chen, Y. Shao, M. H. Engelhard, Z. Nie, J. Xiao, X. Liu, P. V. Sushko, J. Liu, J.-G. Zhang, *J. Am. Chem. Soc.* **2013**, *135*, 4450.
[26] W. Xu, J. Wang, F. Ding, X. Chen, E. Nasybulin, Y. Zhang, J.-G. Zhang, *Energy Environ. Sci.* **2014**, *7*, 513.
[27] J.-T. Yeon, J.-Y. Jang, J.-G. Han, J. Cho, K. T. Lee, N.-S. Choi, *J. Electrochem. Soc.* **2012**, *159*, A1308.

[28] H. Lee, S. M. Dellatore, W. M. Miller, P. B. Messersmith, *Science* **2007**, *318*, 426.
[29] M.-H. Ryou, Y. M. Lee, J.-K. Park, J. W. Choi, *Adv. Mater.* **2011**, *23*, 3066.
[30] M.-H. Ryou, D. J. Lee, J.-N. Lee, Y. M. Lee, J.-K. Park, J. W. Choi, *Adv. Energy Mater.* **2012**, *2*, 645.
[31] S. M. Kang, M.-H. Ryou, J. W. Choi, H. Lee, *Chem. Mater.* **2012**, *24*, 3481.
[32] H. Lee, N. F. Scherer, P. B. Messersmith, *Proc. Natl. Acad. Sci.* **2006**, *103*, 12999.
[33] L. Yin, J. Wang, F. Lin, J. Yang, Y. Nuli, *Energy Environ. Sci.* **2012**, *5*, 6966.
[34] M. Yu, Y. Xu, C. Wang, B. Zhu, Y. Wang, X. Hu, X. Lin, *J. Appl. Polym. Sci.* **2012**, *124*, 5172.
[35] M. Ji, C. Wang, Y. Bai, M. Yu, Y. Wang, *Polym. Bull.* **2007**, *59*, 527.
[36] J. Wang, J. Yang, J. Xie, N. Xu, *Adv. Mater.* **2002**, *14*, 963.
[37] J. Wang, J. Yang, C. Wan, K. Du, J. Xie, N. Xu, *Adv. Funct. Mater.* **2003**, *13*, 487.
[38] X.-g. Yu, J.-y. Xie, J. Yang, H.-j. Huang, K. Wang, Z.-s. Wen, *J. Electroanal. Chem.* **2004**, *573*, 121.
[39] X. Yu, J. Xie, Y. Li, H. Huang, C. Lai, K. Wang, *J. Power Sources* **2005**, *146*, 335.
[40] T. H. Hwang, D. S. Jung, J.-S. Kim, B. G. Kim, J. W. Choi, *Nano Lett.* **2013**, *13*, 4532.
[41] S. S. Zhang, J. A. Read, *J. Power Sources* **2012**, *200*, 77.
[42] S. S. Zhang, D. T. Tran, *J. Power Sources* **2012**, *211*, 169.
[43] J. Fanous, M. Wegner, J. Grimminger, Ä. Andresen, M. R. Buchmeiser, *Chem. Mater.* **2011**, *23*, 5024.
[44] Y.-H. Lee, J.-S. Kim, J. Noh, I. Lee, H. J. Kim, S. Choi, J. Seo, S. Jeon, T.-S. Kim, J.-Y. Lee, J. W. Choi, *Nano Lett.* **2013**, *13*, 5753.
[45] J.-S. Kim, Y.-H. Lee, I. Lee, T.-S. Kim, M.-H. Ryou, J. W. Choi, *J. Mater. Chem. A* **2014**, DOI: 10.1039/c4ta00551a.